https://doi.org/10.1016/j.engstruct.2024.117681

Durability of FRP-to-concrete bonded joints subjected to 110 months accelerated laboratory and field exposure

Zhi-Hao Hao[a,b], Jun-Jie Zeng[c], Guang-Ming Chen[d], Jian-Guo Dai[a,*] and Jian-Fei Chen[b,*]

[a] Department of Civil and Environmental Engineering, The Hong Kong Polytechnic University, Hong Kong, China

[b] Department of Ocean Science and Engineering, Southern University of Science and Technology, Shenzhen, Guangdong, 518055, China.

[c] School of Civil and Transportation Engineering, Guangdong University of Technology, Guangzhou, 510006, China.

[d] State Key Laboratory of Subtropical Building Science, South China University of Technology, Guangdong Province, Guangzhou, 510641, China.

* Corresponding authors

ABSTRACT

Externally bonded fiber reinforced polymer (FRP) composites have been widely used to strengthen existing reinforced concrete (RC) structures. The predominant failure mode in FRP-strengthened RC members is debonding, which is largely dependent on the performance of the FRP-to-concrete interface. Since the FRP-to-concrete bonds are directly exposed to the environment, their durability is crucial to the safety of the strengthened structure. In this study, 84 FRP-to-concrete bonded joints were used, and they were distinguished by the type of FRP reinforcement and adhesives, including carbon FRP (CFRP) plate/Sika30, CFRP plate/Araldite106, CFRP sheet/SW-3C, and glass FRP (GFRP) sheet/Sika330. The performance of FRP-to-concrete interfaces and the corresponding materials (i.e., FRP, adhesives, and concrete), were tested after 8-month, 18-month, 31-month, and 110-month exposure to the wet-dry cycling environment, and 48-month and 110-month exposure to the outdoor environment. The results indicate that bonded joints subjected to the wet-dry cycling environment exhibited more significant degradation compared to those subjected to the outdoor environment. In the wet-dry cycling environment, the CFRP plate/Sika 30 and CFRP sheet/SW-3C

bonded joints exhibited better durability performance with only 3% and 9% reductions in bond strength after 110 months, respectively. In contrast, the CFRP/Araldite106 and GFRP sheet/Sika330 bonded joints exhibited larger reductions in bond strength of 36% and 48%, respectively. Furthermore, failure mode changes were observed as the exposure time increased, and the corresponding degradation mechanisms were discussed.

Keywords: CFRP, GFRP, Durability, FRP-to-concrete interface, Wet-dry cycling environment.

1 INTRODUCTION

Increasing numbers of studies suggested that externally bonded FRP can be a viable solution for the repair and rehabilitation of reinforced concrete (RC) structures, particularly for those in marine environments [1, 2]. This is due to the inherent corrosion resistance of FRP materials, which also serve as a protective layer, mitigating the ingress of chloride ions into the concrete. For FRP-strengthened concrete structures, the FRP-to-concrete interface is the critical element of transferring stresses [3]. But it is vulnerable to debonding, leading to structural failure [4-7]. The performance of the FRP-to-concrete interface has been extensively investigated in recent decades [8-13], which is influenced by various factors, such as concrete strength (f_c'), the stiffness of FRP ($E_f t_f$, E_f and t_f is the elastic modulus and thickness of FRP), effective bond length (L_e), and the width ratio (β_w, the ratio of concrete to FRP width) [14]. Other factors, like the surface conditions of concrete and the properties of the adhesives, also affect the bond performance [15, 16]. To evaluate the bond performance of the FRP-to-concrete interface, several testing methods have been commonly used, including the single shear lap test [17-19], double shear lap test [20-22], direct tension pull-off test [23-25], bending type test [26, 27], and mixed-mode type test [28]. A comprehensive introduction to the testing methods was presented in a previous study [29].

Among these testing methods, the single shear lap test is considered to be the most straightforward, although it requires additional effort to establish suitable facilities. The single shear lap test

specimen consists of five primary components, including (a) concrete; (b) FRP composites; (c) adhesive; (d) FRP-to-concrete interface, and (e) FRP-to-adhesive interface. Chen and Teng [8] indicated six distinct failure modes possible for the FRP-to-concrete interface (Fig. 1), including (1) Concrete failure (CF); (2) Concrete/adhesive interfacial failure (CAF); (3) Adhesive failure (AF); (4) FRP/adhesive interfacial failure (FAF); (5) FRP rupture (FR); (6) FRP delamination (FD).

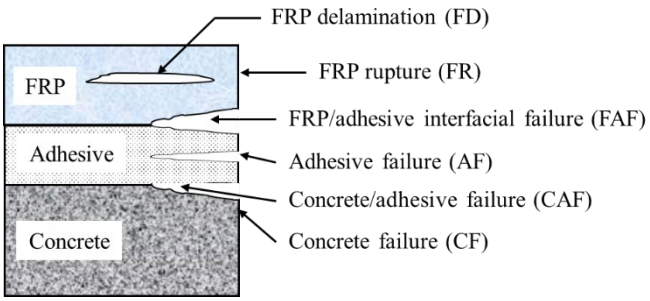

Fig. 1. Schematic of potential failure modes for the FRP-to-concrete interface.

In marine environments, the primary challenge to structures is the corrosion of steel reinforcement caused by moisture and chloride salts [18, 30-33], and these factors also have an adverse effect on the FRP-to-concrete interface [34-36]. Moisture and chloride ions can penetrate into the FRP-to-concrete interface through cracks and voids, causing bond degradation [37-40]. Various studies have investigated the durability of the FRP-to-concrete interface in chloride and moisture environments, as presented in Table 1. The FRP used in these studies included carbon FRP (CFRP), glass FRP (GFRP), and aramid FRP (AFRP), in the form of plates or sheets. The environments included total immersion, wet-dry cycling environment, and salt fog, all of which are commonly experienced by marine structures [41].

Some studies have indicated that the bond strength of the FRP-to-concrete interface can be reduced when subjected to water immersion or wet-dry cycling environments. These studies have investigated the effect of such exposure on different types of FRP, i.e. CFRP sheets [42, 43], GFRP plates [44], and CFRP plates [45]. Table 1 provides a summary of the exposure schemes, which have shown considerable variation. Some studies reported bond strength retentions of over 80% after 150 days [42, 45] or even 416 days [44], while others observed a significant reduction in bond

strength within a shorter exposure period. The reductions in bond strength are attributed to the vulnerability of FRP and adhesive to moisture [46-51]. Dai et al. [52] conducted the pull-off tests and observed that the bond failure shifted from the concrete to the primer-to-concrete interface after exposure to the wet-dry cycling environment. Moreover, Al-Mahmoud et al. [43] observed the debonding surface of the CFRP sheet-to-concrete interface by scanning electron microscope (SEM) and detected the presence of acicular crystals, which they suggested might be sodium carbonate that weakened the adhesive-to-concrete interface.

However, some of the existing studies found that the bond strength exhibited increases at the initial stage of environmental exposure followed by decreases [33, 53]. For instance, Cromwell et al. [33] observed that the bond strength of CFRP plate, CFRP sheet, and GFRP sheet increased to 130.0%, 129.5%, and 110.8% after 125 days of saltwater immersion, then decreased to 93.6%, 113.2%, and 86.6% after 416 days, respectively. In contrast, some studies have reported continuous increases in bond strength during exposure [43, 54, 55], even up to 336 days [56] and 416 days [53]. Silva et al. [53] found that the bond strength of the GFRP sheet-to-concrete interface increased to 142.9% and 131.5% after 416 days of seawater immersion and seawater wet-dry cycles, respectively. The increase in bond strength can be attributed to three primary mechanisms, including post-curing of bonding adhesives leading to increases in adhesive strength; post-hydration of the concrete leading to increases in concrete strength; and plasticization of adhesive leading to stress redistribution along the bonded length.

Without environmental exposure, most FRP-to-concrete interfaces fail due to concrete failure (CF) [8, 57], and failure mode shifts were found after environmental exposure. For instance, Kabir et al. [58] found the failure mode of the CFRP-to-concrete interface changed from a thicker concrete layer to a thinner layer attached to CFRP after wet-dry cycling exposure. Cromwell et al. [33] found the failure mode changed from concrete failure to FRP-to-adhesive interfacial failure or FRP

rupture. Nguyen et al. [59] also observed the failure mode changed from concrete to the concrete-to-adhesive interface. Different failure modes are related to different load-carrying mechanisms. The failure mode changes imply the different degradation of the different load-carrying mechanism, which should be considered in assessing the durability performance of the FRP-to-concrete interface.

It is noteworthy that previous studies have not provided consistent conclusions regarding the long-term performance of the FRP-to-concrete interface, and the tests were limited to relatively short exposure periods, typically less than 500 days. This study aims to investigate the durability of three types of FRP (i.e., CFRP plate, CFRP sheet, and GFRP sheet), four types of adhesives (i.e., SW-3C, Sika330, Sika30, and Araldite106), and four types of FRP-to-concrete joints (i.e., CFRP plate/Sika 30, CFRP plate/Araldite 106, CFRP sheet/SW-3C, and GFRP sheet/Sika 330). These specimens were subjected to wet-dry cycling and outdoor environments for a maximum period of 110 months.

Table 1. Test database of FRP-to-concrete interface.

Authors	FRP	f_{cu} (MPa)	Exposure scheme	Temperature (℃)	Max. time (days)	Bond strength
Cromwell et al. [33]	CFRP plate	30	Immersion in 5% NaCl solution	22	416	Increased to 130% after 125 days and then decreased to 94% after 416 days
	CFRP sheet					Increased to 130% after 125 days and then decreased to 113% after 416 days
	GFRP sheet					Increased to 111% after 125 days and then decreased to 87% after 416 days
Wang and Zhang [42]	CFRP sheet	41	Immersion in artificial seawater	25	150	Decreased to 93% after 150 days
Silva et al. [53]	GFRP sheet	35	Immersion in 5% NaCl solution	25	416	Increased to 143% after 416 days
			Wet-dry cycles in 5% NaCl solution	25		Increased to 132% after 416 days
			5% NaCl salt fog	35		Increased to 106% after 41 days and then decreased to 98% after 416 days
	CFRP sheet	26	5% NaCl salt fog	35		Decreased to 84% after 250 days and then increased to 93% after 416 days
Al-Mahmoud et al. [43]	CFRP sheet	37	Immersion in 3.5% NaCl solution	20	120	Decreased to 52% after 120 days
	CFRP plate					Increased to 105% after 120 days
Al-Tamimi et al. [54]	CFRP plate	50	Immersion in 4% NaCl solution with 3 kN sustained load	25	150	Increased to 109% after 150 days
			Immersion in 4% NaCl solution with 5 kN sustained load			Increased to 116% after 150 days
Wu et al. [60]	AFRP sheet	58	Immersion in 3.5% NaCl solution	25	360	Decreased to 92% after 45 days and then increased to 110% after 360 days
Mukhopadhyaya et al. [55]	GFRP plate	35	Wet-dry cycles in 5% NaCl solution	18	252	Increased to 111% after 252 days
Silva and Biscaia [44]	GFRP sheet	47	Immersion in 5% NaCl solution	22	416	Decreased to 82% after 416 days
Zhang et al. [45]	CFRP plate	47	Immersion in 10% NaCl solution	25	150	Decreased to 87% after 150 days
Hassan et al. [56]	CFRP plate	47	Wet-dry cycles in seawater	25-32	336	Increased to 107% after 336 days

2 EXPERIMENTAL PROGRAM

2.1 Concrete

Standard 150 mm × 300 mm concrete cylinders were used to monitor the compressive strength of concrete over time. The maximum aggregate size of the concrete was 10 mm. The concrete was well cured indoors at 20 ± 2 °C for 28 days. The 7- and 28-day strengths of concrete were 18.8 MPa and 41.0 MPa, respectively.

2.2 FRP

Three types of FRP, which are the most commonly used for strengthening concrete structures, were used: (a) CFRP sheet (CS), with a nominal thickness of 0.167 mm per layer; (b) GFRP sheet (GS), with a nominal thickness of 0.172 mm per layer, and (c) CFRP plate (CP) with a thickness of 1.2 mm. The tensile test of FRP was conducted following the procedure in ASTM D3039. FRP was designed in the dimension of 250 mm × 25 mm. The CS and GS specimens were cut from a single-batch of CS or GS sheet formed by the wet lay-up process. They were fully infiltrated by a well-mixed resin using a roller and then placed in a customized mold and cured for 7 days. The CP specimen was directly cut from pultruded CFRP plates. Before testing, the 56-mm long aluminum tabs were attached at both ends of the FRP to make the anchorages. The tests were performed at a speed of 2 mm/min. For each type of FRP, at least five identical specimens were used.

2.3 Adhesive

Four commercial adhesives were used: SW-3C, Sika330, Sika30, and Araldite106. The tensile test was conducted following the procedure in ASTM D638. Custom-made stainless steel frames were used to cast the epoxy specimens into standard shapes, as shown in Fig. 2. All of the epoxy adhesives were cured indoors at an ambient temperature of 20±2 °C for 7 days. The tests were performed at a speed of 2 mm/min. For each type of adhesive, at least five identical specimens were used.

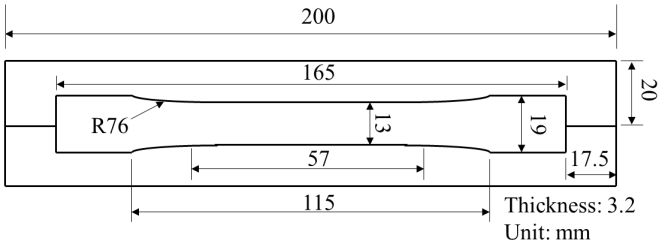

Fig. 2. Dimension of adhesive coupons and molds.

2.4 FRP-to-concrete bonded joint

In this study, the single shear lap test was used [61] to evaluate four types of bonded joints, which were distinguished by the used FRP and adhesive as shown in Table 2. They shared the same dimension (Fig. 3) and used the same concrete that was cured for 28 days. Before installing the FRP sheets/plates, loose and friable materials (e.g., cement laitance) on the concrete surface were removed and cleaned by the chisel and high-pressure air, and a thin layer of well-mixed epoxy primer was applied to the concrete. The bond-free zone was covered by insulating tape to prevent the adhesive from sticking to the concrete. For CFRP and GFRP sheets applied by the wet lay-up method, they were uniformly impregnated with resins (SW-3C for CS; Sika330 for GS) on the primer and leveled with a rubbing roller along the fiber direction. For CFRP plates, they were brushed with sandy paper, solvent wiped, and fully dried before being coated with a layer of adhesive and attached to the concrete. The plates were then pressed uniformly with a roller to squeeze out the excessive adhesive. After one day of curing, insulating tape and excessive adhesives were carefully removed to achieve a clean and regular bond. The specimens were cured indoors (20±2 °C) for over 7 days before being placed in the chamber.

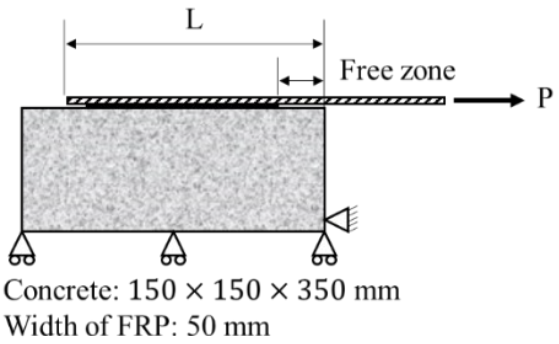

Fig. 3. Dimension of FRP-to-concrete joints.

Table 2. FRP-to-concrete bonded joints.

Type	Thickness (mm)	Adhesive
CFRP plate	1.2 for one layer	Sika30
CFRP plate	1.2 for one layer	Araldite106
CFRP sheet	0.334 for two layers	SW-3C
GFRP sheet	0.344 for two layers	Sika330

To carry out the single shear lap test, a steel frame was manufactured with a platform, load head, hydraulic oil jack, and load cell, as shown in Fig. 4(a). Carefully alignment was performed before testing to ensure the direction of applied force was horizontal and coincided with the centerline of the FRP. 5-mm strain gauges were attached along the centreline of FRP at a spacing of 20 mm from the loaded end towards the free end to obtain accurate local strain distributions, as shown in Fig. 4(b). An additional strain gauge was placed in the free zone of the FRP, 25 mm from the loaded end. Meanwhile, three strain gauges were placed along the transverse direction of FRP at a spacing of 15 mm and a distance of 150 mm from the loaded end to ensure proper load alignment. Apart from the strain gauges, two linear variable displacement transducers (LVDTs) were installed to monitor the relative displacements between FRP and concrete on both the loaded and the free ends. Load application was performed manually using a hydraulic oil jack with a constant increment of 25% of the ultimate load per minute predicted by Chen and Teng [8].

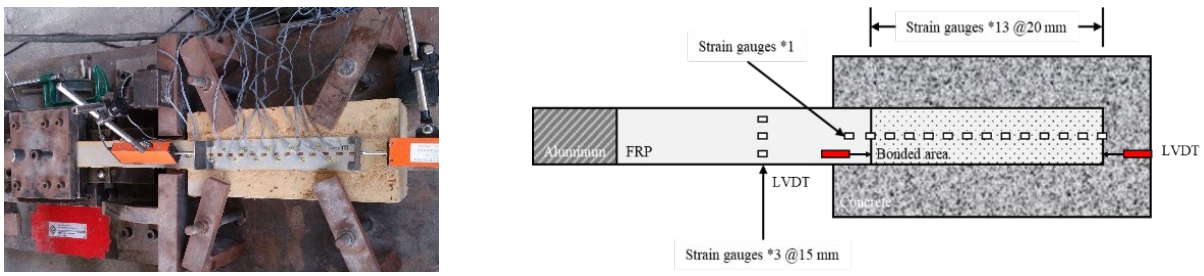

(a) (b)

Fig. 4. Set-up for the single shear lap test.

2.5 Exposure conditions

The specimens in this study were exposed to wet-dry cycling and outdoor environment for up to 110 months, as shown in Fig. 5. Wet-dry cycling was used since it is a common aggressive

environment encountered by marine concrete structures [41]. Each cycle consisted of 16 hours of immersion in 40 ℃ salt water (3.5% sodium chloride), followed by 32 hours of exposure to 40 ℃ dry air. This accelerated exposure scheme enabled efficient drying and wetting of the specimens, and the moderately high temperature accelerated the moisture diffusion while avoiding changing the material degradation mechanisms [62]. The outdoor environment was located in Guangzhou, China, with an average annual temperature of 21.5 ℃ to 22.5 ℃, and the highest and lowest temperatures of 39.1 ℃ and -0.3 ℃. The average annual relative humidity (RH) was 78% to 81%.

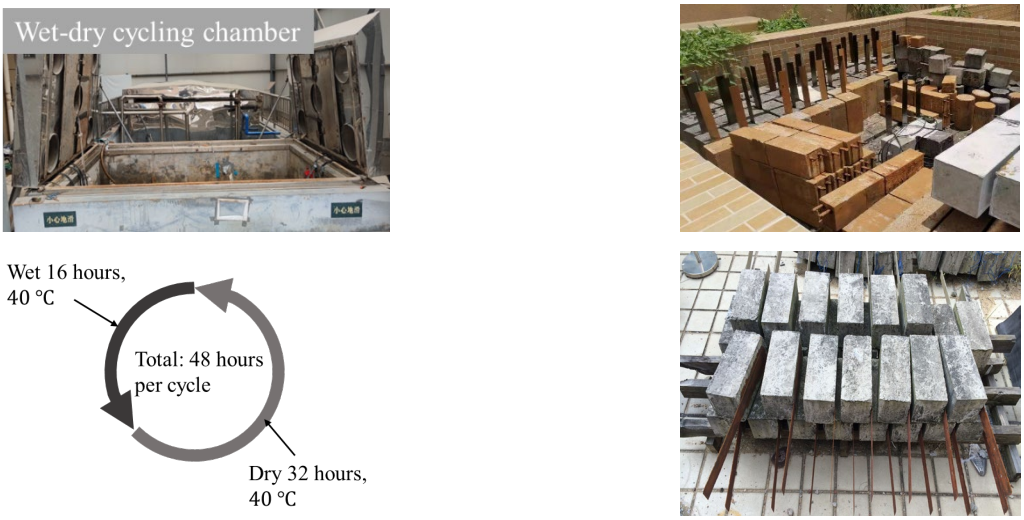

(a) The wet-dry cycling environment (b) The outdoor environment

Fig. 5. The exposure conditions.

Table 3 presents the test program. The wet-dry cycling and outdoor environments are designated by 'L' and 'F', respectively; The specimens are identified with specific labels: 'C' for concrete; 'CP', 'CS', and 'GS' for CFRP plate, CFRP sheet, and GFRP sheet, respectively; 'S330', 'S30', 'SW', and 'A106' for Sika330, Sika30, SW-3C, and Araldite106, respectively; 'CP1B', 'CP2B', 'CSB', and 'GSB' for the FRP-to-concrete bonded joints using CFRP plate/Sika30, CFRP plate/Araldite106, CFRP sheet/SW-3C, and GFRP sheet/Sika330, respectively. The following numbers indicate the exposure duration in months, while the final number represents the number of replicated specimens. For instance, 'L-CSB-8m-1' refers to the first CFRP sheet/SW-3C bonded joint subjected to the wet-dry cycling environment for 8 months.

Table 3. Test program.

Specimens	Exposure duration (months)	
	Wet-dry cycling environment (L)	Outdoor environment (F)
Concrete (C)	1, 8, 18, 31, 110	1, 48, 110
Sika330 (S330)	0, 8, 18, 31, 110	/
Sika30 (S30)	0, 8, 18, 31, 110	/
SW-3C (SW)	0, 8, 18, 31, 110	/
Araldite106 (A106)	0, 8, 18, 31, 110	/
CFRP plate (CP)	0, 8, 18, 31, 110	0, 48, 110
CFRP sheet (CS)	0, 8, 18, 31, 110	0, 48, 110
GFRP sheet (GS)	0, 8, 18, 31, 110	0, 48, 110
CFRP plate/Sika30 (CP1B)	0, 8, /, 31, 110	0, 48, 110
CFRP plate/Araldite106 (CP2B)	0, 8, 18, 31, 110	0, 48, 110
CFRP sheet/SW-3C (CSB)	0, 8, 18, 31, 110	0, 48, 110
GFRP sheet/Sika330 (GSB)	0, 8, 18, 31, 110	0, 48, 110

3 TEST RESULTS

3.1 Concrete

Fig. 6 and Table 4 present the compressive strength and elastic modulus of concrete cylinders over time. In the wet-dry cycling environment, the compressive strength increased by 6.8% after the first 8 months, followed by a gradual decrease. After 110 months, the compressive strength decreased to 40.9 MPa, comparable to the 28-day strength. In the outdoor environment, the compressive strength increased by 38% and 2.3% after 48 months and 110 months, respectively. Notably, no significant degradation of compressive strength was observed in either environment, even after 110 months of exposure.

The elastic modulus of concrete also exhibited no significant degradation in either environment. In the wet-dry cycling environment, the largest elasticity was observed after 31 months, at 29.3 GPa with a 37.6% increase compared to the 28-day concrete. The modulus of elasticity then decreased to

23.5 GPa after 110 months. In contrast, the modulus of elasticity of the concrete in the outdoor environment increased by 11.2% and 16.5% after 48 months and 110 months, respectively.

Table 4. Compressive strength and elastic modulus of the concrete cylinder.

Specimens	Compressive strength (MPa)			Elastic modulus (GPa)		
	Average	COV	Retention	Average	COV	Retention
L-C-1m	41.0	1.85%	100.0%	21.3	4.33%	100.0%
L-C-8m	43.8	0.62%	106.8%	21.4	5.23%	100.5%
L-C-18m	43.1	5.37%	105.1%	/	/	/
L-C-31m	42.3	1.15%	103.2%	29.3	2.75%	137.6%
L-C-110m	40.6	5.59%	99.0%	23.5	8.25%	110.3%
F-C-48m	42.6	2.56%	103.8%	23.7	1.74%	111.2%
F-C-110m	41.9	3.42%	102.3%	24.8	6.77%	116.5%

COV: Coefficient of variation.

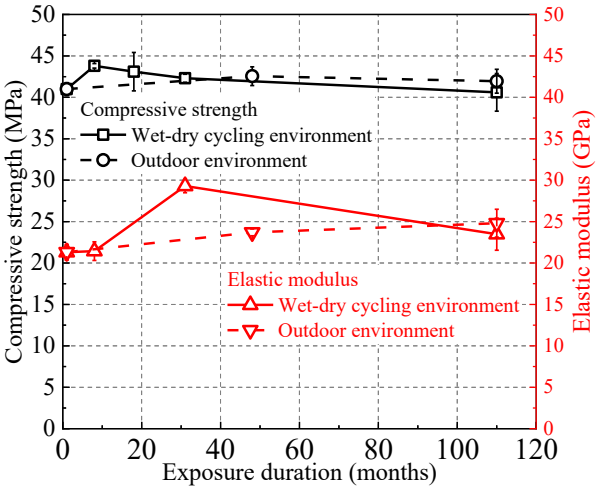

Fig. 6. Changes in concrete properties over time.

3.2 Adhesive

Table 5 presents the tensile strength and elastic modulus of the adhesives over time. Without environmental exposure, SW exhibited the largest tensile strength of 36.4 MPa, followed by S330 and A106 with tensile strengths of 30.9 MPa and 24.4 MPa, respectively, whereas S30 had the smallest tensile strength of 16.2 MPa. Regarding the elastic modulus, S30 had the largest value of 11.4 GPa, followed by S330 of 4.3 GPa and SW of 2.5 GPa. A106 was relatively soft with an elastic modulus of only 0.9 GPa.

Table 5. Tensile strength and elastic modulus of the adhesive.

Specimens	Tensile strength (MPa)			Elastic modulus (GPa)		
	Average	COV	Retention	Average	COV	Retention
L-S330-0m	30.9	9.02%	100.0%	4.3	10.83%	100.0%
L-S330-8m	43.5	4.65%	140.9%	4.7	18.26%	108.9%
L-S330-18m	31.7	5.79%	102.7%	3.3	9.50%	78.3%
L-S330-31m	26.8	10.71%	86.7%	3.1	10.27%	73.3%
L-S330-110m	20.9	13.77%	67.5%	3.1	20.50%	71.8%
L-S30-0m	16.2	5.62%	100.0%	11.4	8.56%	100.0%
L-S30-8m	24.7	12.59%	152.7%	11.1	9.30%	97.3%
L-S30-18m	10.9	29.83%	67.4%	8.0	22.75%	70.0%
L-S30-31m	10.2	14.04%	63.0%	9.8	8.21%	86.2%
L-S30-110m	8.5	9.04%	52.8%	10.0	7.17%	87.4%
L-SW-0m	36.5	9.95%	100.0%	2.5	5.04%	100.0%
L-SW-8m	50.3	12.82%	137.9%	2.9	6.25%	118.2%
L-SW-18m	36.4	7.87%	99.9%	2.5	8.19%	100.9%
L-SW-31m	33.6	9.47%	92.0%	2.4	15.74%	96.0%
L-SW-110m	31.3	11.11%	85.8%	2.2	8.32%	89.7%
L-A106-0m	24.4	6.68%	100.0%	0.9	7.30%	100.0%
L-A106-8m	21.2	11.03%	87.0%	1.3	3.92%	148.8%
L-A106-18m	6.1	23.49%	25.1%	0.9	2.25%	102.0%
L-A106-31m	6.3	26.47%	25.8%	0.8	2.59%	86.5%
L-A106-110m	6.9	28.39%	28.3%	0.7	8.46%	82.8%

COV: Coefficient of variation.

Fig. 7(a) presents the tensile strength change of adhesives in the wet-dry cycling environment. After 8 months, the tensile strength of S330, S30, and SW increased by 40.9%, 52.7%, and 37.9%, respectively. The 7-day strength was taken as the reference strength when the adhesives had not attained their maximum strength. The initial strength increase was attributed to further curing. Subsequently, their tensile strengths quickly decreased to 102.7%, 67.4%, and 99.9%, respectively, after 18 months, followed by a slower decrease rate. After 110 months, the strength retentions of S330, S30, and SW were 67.5%, 52.8%, and 85.8%, respectively. In comparison, A106 exhibited

no initial strength increase, and its tensile strength quickly decreased to 25.1% after 18 months, remaining almost unchanged at 28.3% after 110 months. The glass transition temperature (T_g) of A106 is 45 ℃, which is close to the conditional temperature. This may result in its relatively inferior durability.

Fig. 7(b) presents the elastic modulus change of adhesives in the wet-dry cycling environment, which decreased much less compared to the tensile strength. The elastic moduli of these adhesives exhibited significant changes within the first 18 months and then became stable. After 110 months, the elastic moduli of S330, S30, SW, and A106 were retained at 71.8%, 87.4%, 89.7, and 82.8% of their initial values, respectively,

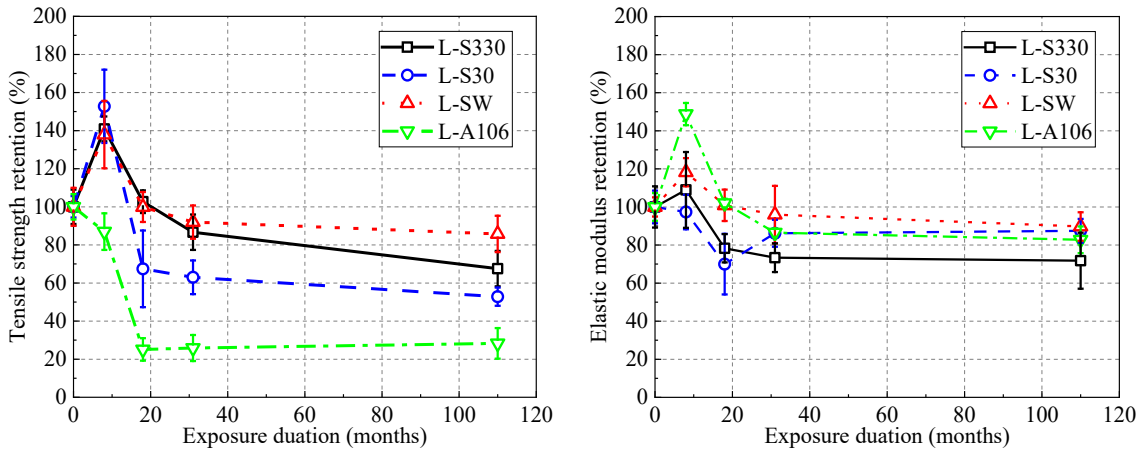

(a) Tensile strength (b) Elastic modulus

Fig. 7. Changes in adhesive properties over time.

3.3 FRP

Table 6 presents the tensile strength and elastic modulus of the FRP over time. Without exposure, CS exhibited the largest tensile strength and elastic modulus, followed by CP, while GS had the smallest tensile strength and elastic modulus.

Fig. 8 presents the tensile strength of FRP in the wet-dry cycling environment and outdoor environment. The tensile strength of GS decreased rapidly to 51.1% after 8 months of exposure in the wet-dry cycling environment, followed by a slower decreasing rate. After 110 months, the

tensile strength retention of GS was 47.2%. Similar degradation trends were observed for GS in the outdoor environment, where the tensile strength decreased rapidly to 62.6% after 48 months, and then decreased gradually to 61.4% after 110 months. The outdoor environment was found to be less aggressive than the wet-dry cycling environment for GS.

Table 6. Tensile strength and elasticity of FRP.

Specimens	Tensile strength (MPa)			Elastic modulus (GPa)		
	Average	COV	Retention	Average	COV	Retention
L-CP-0m	2398	0.45%	100.0%	167	0.45%	100.0%
L-CP-8m	2694	3.77%	112.3%	161	3.77%	96.5%
L-CP-18m	2544	5.24%	106.1%	165	5.24%	98.8%
L-CP-31m	2313	8.25%	96.4%	168	8.25%	100.5%
L-CP-110m	1996	9.60%	83.2%	160	9.60%	95.9%
F-CP-48m	2865	2.90%	119.4%	162	3.05%	97.1%
F-CP-110m	2296	3.28%	95.7%	165	2.26%	98.9%
L-CS-0m	4585	5.47%	100.0%	236	4.08%	100.0%
L-CS-8m	4860	7.17%	106.0%	239	8.51%	101.4%
L-CS-18m	5016	2.33%	109.4%	248	9.11%	104.9%
L-CS-31m	4711	2.77%	102.8%	242	9.80%	102.7%
L-CS-110m	4257	7.25%	92.8%	242	4.72%	102.5%
F-CS-48m	4853	4.61%	105.8%	250	6.70%	105.9%
F-CS-110m	4306	6.51%	93.9%	252	4.68%	106.8%
L-GS-0m	1552	2.36%	100.0%	113	4.23%	100.0%
L-GS-8m	794	19.52%	51.1%	121	1.65%	107.1%
L-GS-18m	750	6.58%	48.3%	110	2.87%	97.8%
L-GS-31m	772	14.44%	49.8%	109	6.82%	96.7%
L-GS-110m	732	7.21%	47.2%	108	1.86%	95.2%
F-GS-48m	972	12.42%	62.6%	120	5.21%	106.4%
F-GS-110m	953	14.68%	61.4%	108	4.63%	95.6%

COV: Coefficient of variation.

In comparison, CFRP composites demonstrated relatively better durability, with CS exhibiting the best performance. CS showed slight strength increases during the initial exposure stage in both environments. After 110 months, the tensile strength retentions of CS in the wet-dry cycling

environment and outdoor environment were 92.8% and 93.9%, respectively. For CP, the tensile strength also slightly increased initially, and after 110 months, the tensile strength decreased to 83.2% in the wet-dry cycling environment, much larger than that of CS, while it decreased to 95.7% in the outdoor environment, slightly smaller than that of CS. Both CS and CP used carbon fiber, and the larger degradation of CP was attributed to the matrix resin, which is susceptible to degradation by moisture particularly in the wet-dry cycling environment.

In terms of elastic modulus, CS had the largest value of 236 GPa, followed by CP and GS of 167 GPa and 113 GPa, respectively. The elastic modulus of FRP did not exhibit significant degradation in either environment.

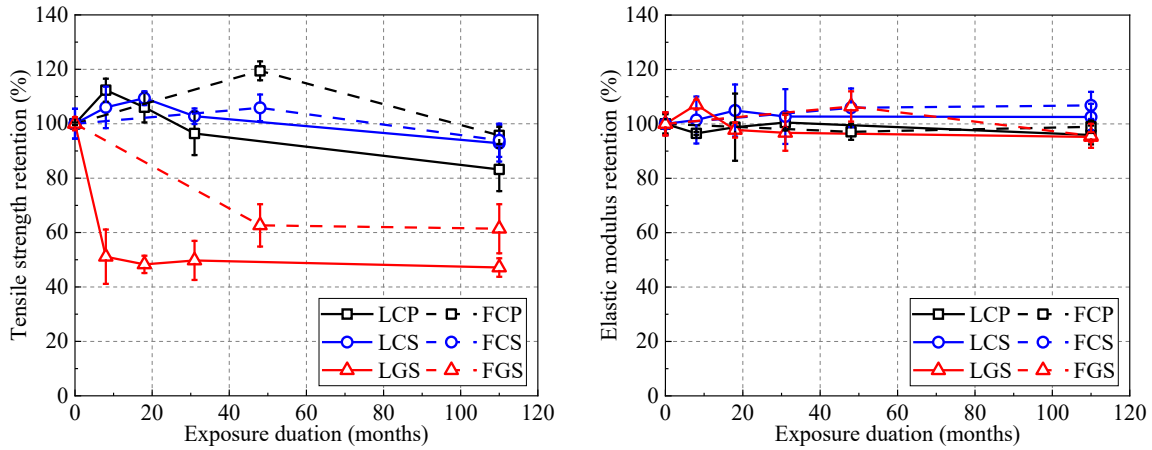

(a) Tensile strength (b) Elastic modulus

Fig. 8. Changes in FRP properties over time.

3.4 FRP-to-concrete bonded joints

3.4.1 Failure modes

Chen and Teng [8] identified six failure modes for FRP-to-concrete bonded joints, as shown in Fig. 1. In this study, all failure modes were observed except for CAF. The failure modes were presented in Table 7 and Appendix A1. Without environmental exposure, concrete failure was commonly observed. The failure process initiated with visible concrete cracking near the loaded end. As the load increased, the FRP began to debond from the cracked concrete at the loaded end, and the cracks then propagated towards the far end of the FRP, ultimately resulting in complete brittle

debonding. As the exposure time increased, failure mode changes were observed in some specimens. Different failure modes are associated with different mechanisms, and these failure mechanisms are related to the properties of different components (i.e., adhesive, FRP, concrete, and their interfaces). Failure mode changes indicate changes in the mechanisms, which are attributed to the different degradation of each component.

CP1B

Figs. 9(a) and 9(b) present that the failure modes of L-CP1B changed from CF to FD. In the wet-dry cycling environment, the concrete property remained stable, while the CFRP plate was vulnerable to moisture, which resulted in a reduction in the interlaminar shear strength of the CFRP plates. Therefore, the load corresponding to concrete crushing did not exhibit much decrease, while that corresponding to CFRP delamination was reduced over time. Once the load for CFRP delamination became lower than that for concrete crushing, the failure mode transitioned from CF to FD. In contrast, after exposure to the outdoor environment, F-CP1B exhibited no failure mode change, as shown in Fig. 9(c). It was attributed to the relatively less moisture in the outdoor environment, which did not cause significant degradation of CFRP plates, and hence the load for the CFRP delamination did not decrease.

(a) CP1-0m

(b) L-CP1-110m

(c) F-CP1-110m

Fig. 9. The failure mode of CP1B.

CP2B

Figs. 10(a)-(c) present that L-CP2B exhibited failure mode changes from CF to AF after 8 months and then to FAF after 110 months in the wet-dry cycling environment. This suggests that the load corresponding to CF, AF, and FAF alternated as the smallest over time, and the A106 and CFRP plate-to-A106 interface exhibited obvious degradation. Compared with L-CP1B (S30), L-CP2B

(A106) used the same materials except for the adhesive. It suggests that the durability of A106 is not as good as S30, which can be also confirmed by the adhesive durability tests. The failure modes of F-CP2B also changed from CF to FAF, as presented in Fig. 10(d), which indicated that the outdoor environment also adversely affected the strength of the A106 and CFRP plate-to-A106 interface.

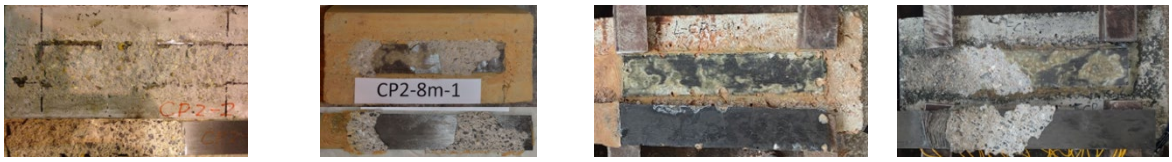

(a) CP2-0m (b) L-CP2-8m (c) L-CP2-110m (d) F-CP2-110m

Fig. 10. The failure mode of CP2B.

CSB

Fig. 11 presents that the failure modes exhibited no change in either L-CSB or F-CSB. All specimens failed due to concrete crushing, suggesting that the deterioration of the CFRP sheet, SW adhesive, and interface was relatively small, resulting in no significant reduction in the loads corresponding to these failure mechanisms.

(a) CS-0m (b) L-CS-110m (c) F-CS-110m

Fig. 11. The failure mode of CP2B.

GSB

L-GSB and F-GSB failed due to concrete crushing before exposure. After exposure to both environments, the failure modes changed to GFRP rupture, as shown in Fig. 12. It was due to a significant decrease in the tensile strength of the GFRP sheet, as proved by the FRP durability tests.

(a) GS-0m (b) L-GS-31m (c) F-GS-110m

Fig. 12. The failure mode of GSB.

Table 7. Results of single-layer pullout test.

Specimens	Ultimate loads (kN)			Failure modes		
	Ave	COV	Retention	1	2	3
L-CP1B-0m	30.2	2.50%	100.0%	CF/AF	CF	AF
L-CP1B-8m	34.3	6.64%	113.7%	CF	CF	CF
L-CP1B-18m	/	/	/	/	/	/
L-CP1B-31m	33.8	5.22%	112.1%	CF	/	FD
L-CP1B-110m	29.4	6.47%	97.6%	FD	FD	FD
F-CP1B-48m	33.0	0.42%	109.4%	CF	CF	CF
F-CP1B-110m	27.7	6.70%	91.8%	AF	CF	AF
L-CP2B-0m	25.9	1.40%	100.0%	/	CF	CF
L-CP2B-8m	26.6	2.52%	102.8%	AF	AF	AF
L-CP2B-18m	19.3	0.91%	74.5%	AF	AF	/
L-CP2B-31m	20.9	13.65%	80.9%	FAF	FAF	CF
L-CP2B-110m	16.6	11.65%	64.1%	FAF	FAF	/
F-CP2B-48m	33.0	5.84%	127.5%	CF	FAF	CF
F-CP2B-110m	22.1	11.37%	85.6%	CF	AF	AF
L-CS-0m	26.9	2.96%	100.0%	CF	CF	CF
L-CS-8m	26.0	8.37%	96.8%	CF	CF	CF
L-CS-18m	25.0	2.55%	92.8%	CF	/	CF
L-CS-31m	25.1	2.57%	93.2%	CF	CF	CF
L-CS-110m	24.4	/	90.6%	CF	/	/
F-CS-48m	29.3	14.34%	109.1%	CF	CF	CF
F-CS-110m	29.5	8.15%	109.9%	CF	CF	CF
L-GS-0m	14.6	5.58%	100.0%	CF	CF	CF
L-GS-8m	12.2	11.86%	83.6%	FR	FR	FR
L-GS-18m	12.3	5.62%	84.1%	FR	FR	/
L-GS-31m	9.2	22.26%	63.3%	FR	FR	FR
L-GS-110m	7.6	3.43%	52.0%	FR	FR	/
F-GS-48m	12.5	7.20%	85.9%	FR	FR	FR
F-GS-110m	11.3	2.98%	77.1%	FR	FR	FR

'/' represents missing data due to defects in the specimens

3.4.2 Bond strength

Fig. 13 and Table 7 present the bond strengths of the specimens. Without exposure, the bond strength of CP1B was the largest, followed by CP2B and CSB. The bond strength of GSB was the smallest. According to Chen and Teng [8], the bond strength has a positive correlation with FRP stiffness ($E_p t_p$), as shown in Eq. 1.

$$P_u = 0.427\beta_P\beta_L\sqrt{f_c'}b_pL_e \quad (1a)$$

$$L_e = \sqrt{\frac{E_p t_p}{\sqrt{f_c'}}} \quad (1b)$$

$$\beta_L = \begin{cases} 1 & if\ L \geq L_e \\ \sin\frac{\pi L}{2L_e} & if\ L < L_e \end{cases} \quad (1c)$$

where, P_u is the ultimate load; b_p is the FRP width; f_c' is the cylinder compressive strength of concrete; β_P and β_L are two parameters considering the width ratio of FRP to concrete and effective bond length, respective; and L_e is the effective bond length. The stiffness values of CP, CS, and GS were 200 kN/mm, 79 kN/mm, and 39 kN/mm, respectively. As the values of CS and GS were lower than that of CP, the bond strength of the CSB and GSB was lower. For CP1B and CP2B, they both used the CFRP plate but different adhesives, which led to different bond strengths. The A106 adhesive used in CP2B, due to the lower elasticity, resulted in a longer effective bond length, possibly exceeding the available bond length leading to lower bond strength compared to CP1B.

After exposure to the wet-dry cycling environment, different specimens exhibited different degradation. L-GSB exhibited the most significant degradation due to the poor durability of the GFRP sheet, and the bond strength was reduced to 52.0% after 110 months. The bond strength of L-CP2B also exhibited substantial decreases to 64.1% after 110 months, mainly due to the poor durability of the A106 adhesive. The degradation of the adhesive was found to affect the bond strength. In contrast, the bond strength of L-CP1B increased by 13.7% after 8 months, then gradually decreased to 97.6% retention after 110 months. The increase in bond strength was attributed to the post-curing of the S30 adhesive, as confirmed by the adhesive test. The bond strength of L-CSB also exhibited relatively small reductions to 90.6% after 110 months.

In the outdoor environment, the specimens showed less degradation. F-GSB exhibited relatively more degradation among the specimens, with a bond strength retention of 77.1% after 110 months. F-CP1B and F-CP2B initially exhibited increases in bond strength before gradually decreasing to

91.8% and 85.6% after 110 months, respectively. F-CSB exhibited the best durability performance, with a 9.9% increase in bond strength after 110 months.

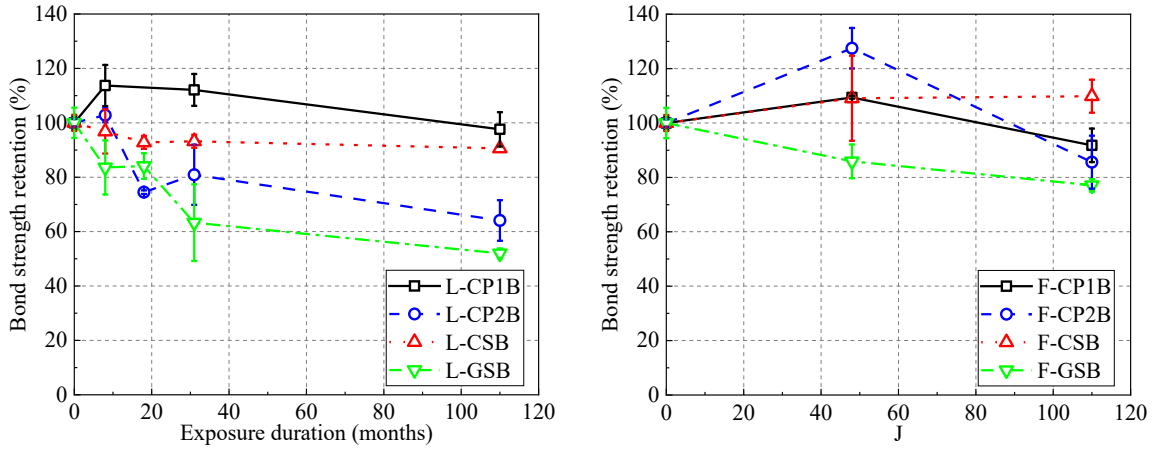

(a) (b)

Fig. 13. Changes of FRP-to-concrete bond strength with exposure time.

4 DISCUSSIONS

4.1 Envelope of bond strength

This study observes the failure mode changes of bonded joints over time, which was also observed in previous research [33, 58, 63]. Different failure modes are associated with different failure mechanisms, and different failure mechanisms are affected by the properties of different components (i.e., FRP, adhesive, and their interfaces). Specifically, the bond strength of bonded joints that failed due to CF is dependent on concrete strength, while FAD failures depend on FRP-to-adhesive interfacial strength. FD and FR failures are dependent on the interlaminar and tensile strength of FRP, respectively, and AF failure depends on the adhesive property.

Fig. 14 illustrates the schematic representation of loads corresponding to various failure modes. The bond strength of the specimens is determined by the minimum value of these loads:

$$P_m(t) = \min\{P_{m,1}(t), P_{m,1}(t), \dots, P_{m,i}(t)\} \quad (2)$$

where $P_m(t)$ represents bond strength at time t and $P_{m,i}(t)$ represents the load corresponding to failure mode (i) at time t, i.e., CF, CAF, AF, and so on. These loads follow different trends as the exposure time increases, resulting in the change in failure mode corresponding to the minimum load

with exposure time. For instance, Fig. 14(a) shows the failure mode change from CF to FD due to a decrease in the interlaminar shear strength of FRP. Fig. 14(b) shows the failure mode change from CF to AF and then FAD, which indicates that the adhesive and the FRP-to-adhesive interface sequentially become the weakest over time. Fig. 14(c) shows the failure mode keeps CF as other components exhibit better degradation resistance. Fig. 14(d) shows the failure mode change from CF to FR due to the poor durability of FRP.

Therefore, the long-term strength of the FRP-to-concrete interface should be determined by the envelope enclosed by the lower bound of the loads corresponding to different failure modes

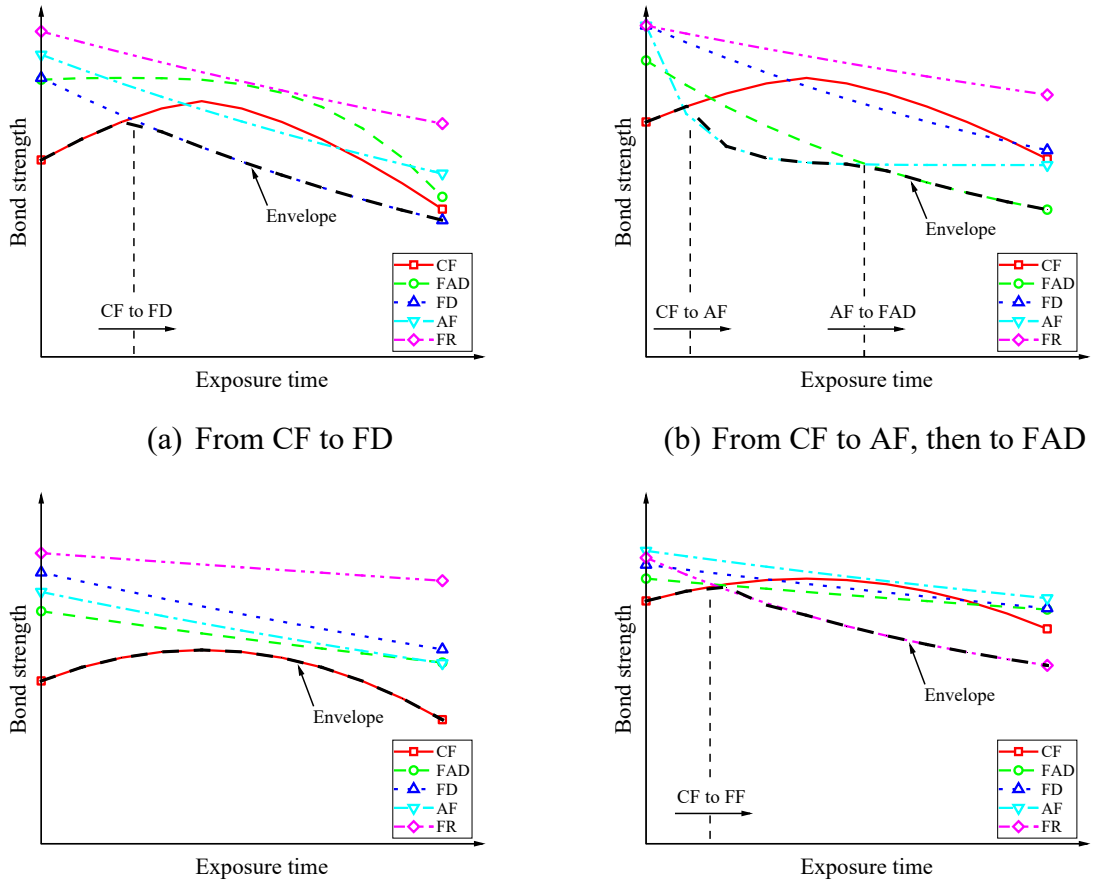

Fig. 14. Schematic of possible failure mode shifts.

4.2 Bond-slip model

According to Dai et al. [9], the relationship between the axial strain ($\varepsilon(x)$) in the FRP and the interfacial slip ($\delta(x)$) between the FRP and the concrete at any location can be expressed as follows:

$$\varepsilon(x) = f[\delta(x)] \tag{3}$$

By assuming that the bond stress and slip relationship is unique along the FRP-to-concrete interface, Eq. 3 is valid for all locations of a sufficiently long bond length [12]. The following exponential expression was found to represent $f[\delta(x)]$ with sufficient accuracy [9]:

$$\varepsilon(x) = f[\delta(x)] = A\left(1 - e^{-B\delta(x)}\right) \tag{4}$$

where A and B are parameters to be determined by regression of test results. The physical meaning of A is the maximum strain of the FRP if its bond length is longer than the effective bond length. B can be regarded as the brittleness index that controls the shape of the bond-slip curve: a larger value of B corresponds to steeper ascending and descending branches. Noting that

$$\tau(x) = \frac{E_f t_f}{1+\alpha}\frac{d\varepsilon(x)}{dx} \tag{5}$$

and

$$\varepsilon(x) = \frac{d\delta(x)}{dx} \tag{6}$$

where $E_f t_f/(1+\alpha)$ is the stiffness ratio of the bonded joint and $\alpha = E_f t_f b_f / E_c t_c b_c$; b_f and b_c are the width of FRP and concrete; t_f and t_c are the thickness of FRP and concrete; and E_f and E_c are the elastic moduli of FRP and concrete, respectively. Combining these equations yields the following equation for the bond-slip model of FRP-to-concrete interfaces:

$$\tau(x) = A^2 B \frac{E_f t_f}{1+\alpha}\left(e^{-B\delta(x)} - e^{-2B\delta(x)}\right) \tag{7}$$

If G_f is used to denote the interfacial fracture energy, which is the area underneath the bond stress-slip curve, the following expression can be obtained:

$$A = \sqrt{\frac{2G_f}{E_f t_f}(1+\alpha)} \tag{8}$$

By substitution of Eq. 8 into Eq. 7, the bond-slip model can be rewritten as:

$$\tau(x) = 2G_f B\left(e^{-B\delta(x)} - e^{-2B\delta(x)}\right) \tag{9}$$

If a sufficient long bond length is provided so that the loaded end slip is large enough, the bond strength can be calculated using the following equation:

$$P_m = b_f \sqrt{2G_f \frac{E_f t_f}{1+\alpha}} \tag{10}$$

Since the FRP width is smaller than the concrete in this study, the force is transferred to the concrete in the vicinity of both sides of FRP, leading to a nonuniform stress distribution across the width of the concrete. Chen and Teng [8] proposed a width factor, β_w, to consider this effect. Therefore, Eq. 10 can be modified as:

$$P_m = \beta_w b_f \sqrt{2G_f \frac{E_f t_f}{1+\alpha}} \tag{11}$$

$$\beta_w = \sqrt{\frac{2 - b_f/b_c}{1 + b_f/b_c}} \tag{12}$$

Based on Eq. 7, the maximum bond stress (τ_m) can be obtained as follows:

$$\tau_m = 0.5BG_f \tag{13}$$

Based on the above equations, the strain distribution of FRP under pullout load P and long bond length L can be expressed as [12]:

$$\varepsilon(x) = \frac{A}{1+e^{BA(L-x)\frac{P_m - P}{P}}} \tag{14}$$

If the strain distributions at different load levels and different locations $\varepsilon_{i,j}$ are obtained from tests ($i = 1, \dots, m$ and $i = 1, \dots, n$, where m and n denote the number of load level and strain gauge), the values of B and A (G_f or $P_{m,pred}$) can be determined through least-square minimization of the difference between the test and predicted strain values with the use of the following equation:

$$e = \sum_{i=1}^{m} \sum_{j=1}^{n} \left[\left(\varepsilon_{i,j}\right)_{pred} - \left(\varepsilon_{i,j}\right)_{test} \right]^2 \tag{15}$$

The bonded joint specimens under the wet-dry cycling environment were analyzed except for the L-GSB since most of the L-GSB failed due to GFRP rupture, which prevented the local behavior of L-GSB from being determined. The parameters obtained by the regression are listed in Table 8. Fig.

15 presents the comparisons of unexposed specimens between experimental strain distributions in FRP and analytical results. The rather good agreement indicates that the proposed bond-slip model is reliable for the FRP-to-concrete joints without exposure. The other regression results are presented in Appendix A2.

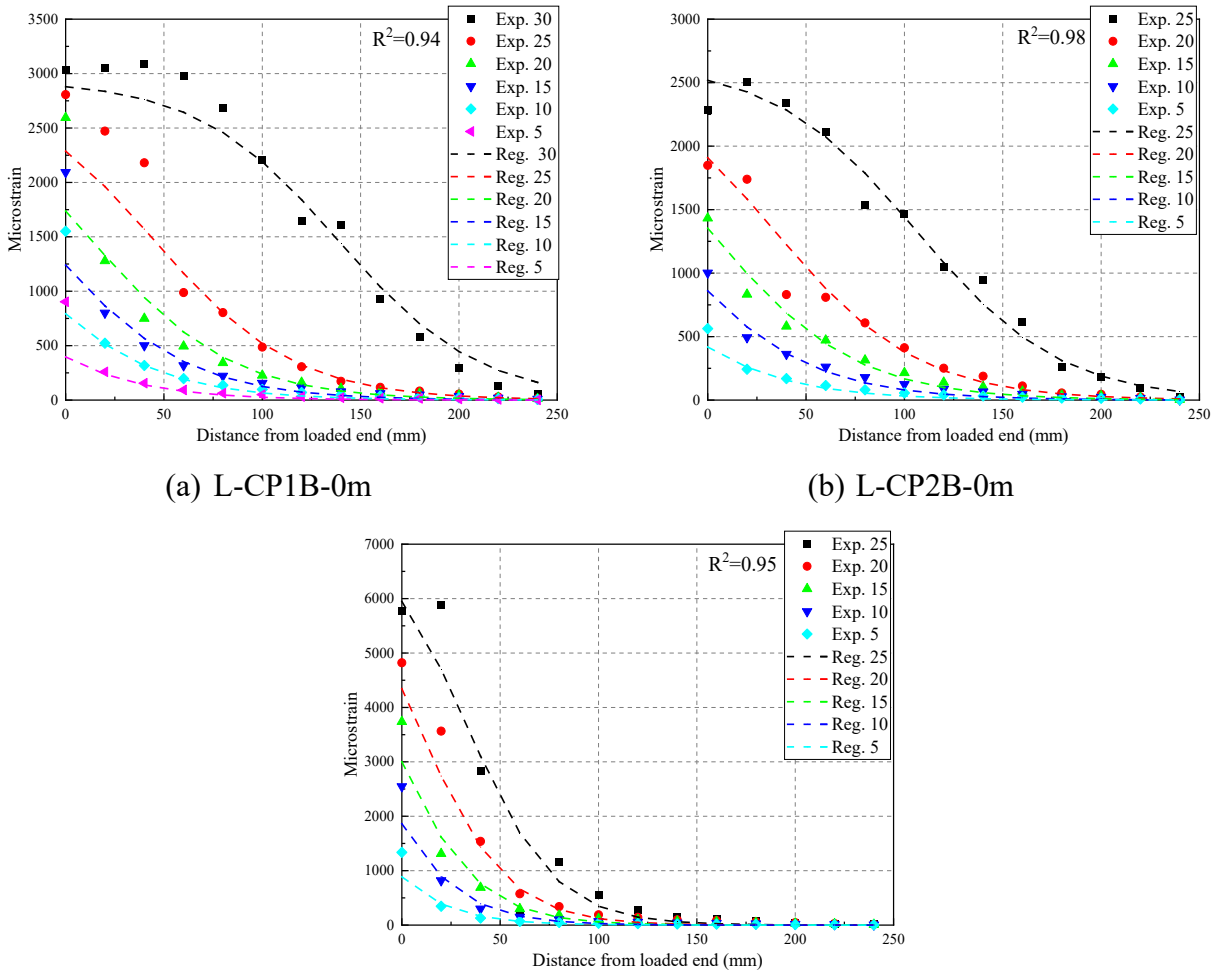

(a) L-CP1B-0m (b) L-CP2B-0m

(c) L-CSB-0m

Fig. 15. Comparison between experimental and regressed strain distribution in FRP.

L-CP1B

Once parameters *A* and *B* are obtained, local bond stress-slip curves can be plotted according to Eq. 9, as shown in Fig. 16. Fig. 16(a) shows the local bond stress-slip curve for L-CP1B in the wet-dry cycling environment. In the first 8 months, the initial stiffness of the curves remains relatively unchanged, after which stiffness decreases with increasing exposure time. The failure modes of L-CP1B-0m and L-CP1B-8m were due to concrete failure, while those of L-CP1B-31m and L-CP1B-

110m were predominantly due to FRP delamination. The failure mode change may lead to decreases in curve stiffness.

The maximum bond stress, calculated using regressed parameters, increases from 4.84 MPa to 5.41 MPa after 8 months before decreasing. The interfacial fracture energy demonstrates a similar pattern to the maximum bond stress. The decrease in maximum bond stress and interfacial fracture energy is due to the failure mode change.

L-CP2B

Fig. 16(b) presents the local bond stress-slip curve for L-CP2B, showing a complex variation in bond behavior due to the failure mode change after exposure. Unexposed specimens failed due to concrete failure, resulting in a steeper ascending branch. After 8 and 18 months, the stiffnesses decreased considerably and the failure modes of those specimens changed to adhesive failure. Furthermore, as exposure time increased, the stiffnesses decreased even more and the failure modes changed to FRP-to-adhesive interfacial failure.

The maximum bond stress of L-CP2B continuously decreased from 3.84 MPa to 0.84 MPa after 110 months. The interfacial fracture energy also decreased to 0.39 MPa after 110 months of exposure.

L-CSB

Fig. 16(c) shows the local bond stress-slip curve for L-CSB. The stiffnesses of the ascending branches were similar before and after exposure and the failure modes exhibited no change. The values of A slightly decreased after environmental exposure, indicating an increased brittleness of failure. Compared to other types of joints, L-CSB has the largest maximum bond stress of 6.03 MPa before exposure, with slight reductions over time.

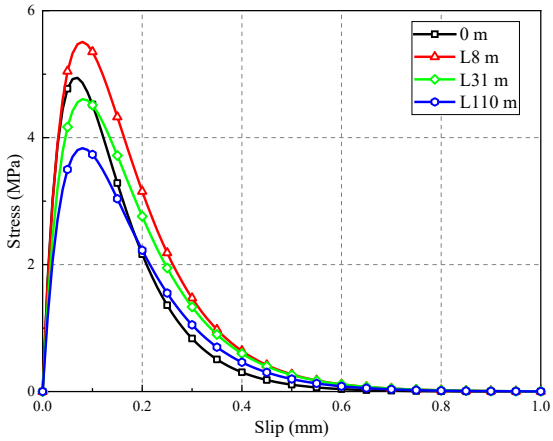

(a) L-CP1B

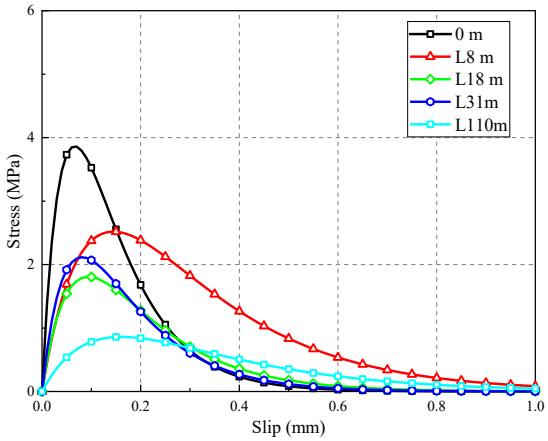

(b) L-CP2B

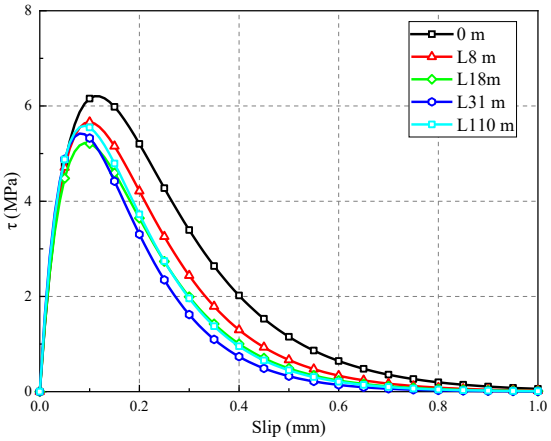

(c) L-CSB

Fig. 16. Bond stress-slip curves.

Table 8. Regression results of strain distribution on FRP.

Specimen	τ_m (MPa)	A (10^{-6})	B (mm^{-})	G_f (N/mm)	$P_{m,pred}$ (kN)	$P_{m,pred}/P_{m,test}$
L-CP1B-0m	4.84	3100	10.4	0.93	30.1	1.00
L-CP1B-8m	5.41	3562	8.77	1.23	34.6	1.01
L-CP1B-31m	4.59	3313	8.48	1.07	32.3	0.96
L-CP1B-110m	4.02	2987	8.68	0.84	28.2	0.96
L-CP2B-0m	3.84	2777	10.44	0.74	26.5	1.02
L-CP2B-8m	2.47	3310	4.79	1.03	31.2	1.17
L-CP2B-18m	1.77	2260	7.37	0.48	21.3	1.10
L-CP2B-31m	2.09	2273	8.53	0.51	22.2	1.06
L-CP2B-110m	0.84	2039	4.31	0.39	19.2	1.16
L-CS-0m	6.03	7133	6.04	1.99	27.9	1.04
L-CS-8m	5.53	6331	6.99	1.59	25.1	0.96
L-CS-18m	5.39	5887	7.46	1.43	24.2	0.97

L-CS-31m	5.38	5663	8.37	1.29	22.7	0.91
L-CS-110m	5.54	5964	7.77	1.43	23.9	0.98

Fig. 17 compares the predicted bond strength obtained from the proposed bond-slip model with the bond strength from tests. Most prediction deviations of L-CP1B and L-CSB are within 5%, indicating the reliability of the proposed model for these specimens regardless of the exposure. The prediction deviation of L-CP2B without exposure is only 2%, but the deviations increase after exposure, attributed to the failure mode change to adhesive failure or FRP-to-adhesive interfacial failure. The proposed model is thus not suitable for those failure mechanisms.

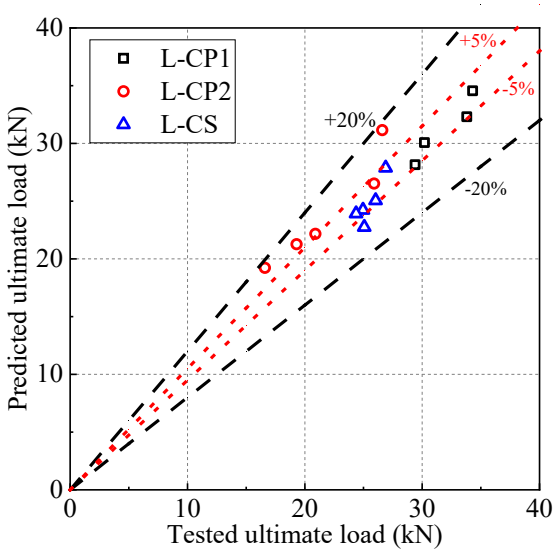

Fig. 17. Comparisons between predicted and test ultimate loads of FRP-to-concrete joints.

5 CONCLUSIONS

This study conducted durability tests on concrete, FRP, adhesive, and FRP-to-concrete interface in wet-dry cycling and outdoor environments. The following concluding remarks and recommendations can be drawn:

(1) The concrete was relatively stable under both environments. The compressive strength increased slightly after exposure due to post-curing and then slowly decreased;

(2) Four commercial adhesives were tested (i.e., SW-3C, Sika330, Sika30, and Araldite106). The tensile strength increased slightly after exposure due to post-curing except for Araldite106. Then, the strength decreased quickly. As the exposure time further increased, the decreasing rate

slowed down. In comparison, the durability performance from good to bad ranked as SW-3C, Sika330, Sika30, and Araldite106. The glass transition temperature (Tg) of A106 is 45 ℃, which is close to the conditional temperature. This may result in its relatively inferior durability.

(3) Three types of FRP were investigated (i.e., CFRP plate, CFRP sheet, and GFRP sheet). GFRP sheet exhibited the most severe degradation compared with other CFRP composites. CFRP plate presented inferior durability than CFRP sheet under the wet-dry cycling environment due to the presence of moisture. All FRP exhibited more degradation in the wet-dry cycling environment than in the outdoor environment;

(4) Four types of FRP-to-concrete joints were investigated, which were distinguished by FRP and adhesive, including CFRP plate/Sika 30, CFRP plate/Araldite 106, CFRP sheet/SW-3C, and GFRP sheet/Sika 330. Failure mode changes were observed in some specimens after exposure. This study suggests that the long-term strength of the FRP-to-concrete interface should be determined by the low-bound of the loads corresponding to different failure mechanisms;

(5) In the wet-dry cycling environment, the bonded joints of CFRP plate/Araldite 106 and GFRP sheet/Sika 330 exhibited significant degradation, with 52.0% and 64.1% bond strength retention after 110 months, respectively, which is due to the inferior durability of the Araldite106 and GFRP sheet. The bonded joints of CFRP plate/Sika 30 and CFRP sheet/SW-3C showed better durability, with 97.6% and 90.6% bond strength retention after 110 months, respectively;

(6) The bonded joints in the outdoor environment exhibited much less degradation than those in the wet-dry cycling environment. The bonded joints of CFRP plate/Sika 30, CFRP plate/Araldite 106, CFRP sheet/SW-3C, and GFRP sheet/Sika 330 had 91.8%, 85.6%, 109.9%, and 77.1% strength retention after 110 months, respectively.

ACKNOWLEDGMENTS

The writers gratefully acknowledge that the present work presented has been financially supported by the Research Grants Council of Hong Kong through General Research Fund (Project code:

516509) and Theme-based Research Scheme (Project code: T22-502/18-R). The first author would like to acknowledge the funding support for the Joint Ph.D. Scheme between Southern University of Science and Technology and The Hong Kong Polytechnic University. The authors are also thankful to Prof. Jin-Guang Teng for his advice in planning the experimental program, and Prof. Wang Xiaohui and Mr. Dian-Yu Sun, for their assistance in the experimental work. The exposure and dry-wet-dry cycling tests had been carried out in the structural lab and exposure site of Guangdong University of Technology (GDUT), the experimental work/help from the former postgraduates students of GDUT, Mr. Liu Weinan and Mr. Wu Zhenkai are noted and appreciated.

REFERENCES

[1] Xie J.H., Hu R.L. Experimental study on rehabilitation of corrosion-damaged reinforced concrete beams with carbon fiber reinforced polymer. Construction and Building Materials. 2013;38:708-16.

[2] Chotickai P., Somana S. Performance of CFRP-Strengthened Concrete Beams after Exposure to Wet/Dry Cycles. Journal of Composites for Construction. 2018.

[3] Teng J.G., Chen J.F. Mechanics of debonding in FRP-plated RC beams. Proceedings of the Institution of Civil Engineers - Structures and Buildings. 2009;162:335-45.

[4] Smith S.T., Teng J.G. FRP-strengthened RC beams. I: review of debonding strength models. Engineering Structures. 2002;24:385-95.

[5] Smith S.T., Teng J.G. FRP-strengthened RC beams. II: assessment of debonding strength models. Engineering Structures. 2002;24:397-417.

[6] Teng J.G., Smith S.T., Yao J., Chen J.F. Intermediate crack-induced debonding in RC beams and slabs. Construction and building materials. 2003;17:447-62.

[7] Chen G., Teng J., Chen J. Finite-element modeling of intermediate crack debonding in FRP-plated RC beams. Journal of composites for construction. 2011;15:339-53.

[8] Chen J.F., Teng J.G. Anchorage strength models for FRP and steel plates bonded to concrete. Journal of structural engineering. 2001;127:784-91.

[9] Dai J., Ueda T., Sato Y. Development of the nonlinear bond stress–slip model of fiber reinforced plastics sheet–concrete interfaces with a simple method. Journal of composites for construction. 2005;9:52-62.

[10] Wu Y.-F., Jiang C. Quantification of bond-slip relationship for externally bonded FRP-to-concrete joints. Journal of Composites for Construction. 2013;17:673-86.

[11] Wu Z., Islam S., Said H. A three-parameter bond strength model for frp—concrete interface. Journal of reinforced plastics and composites. 2009;28:2309-23.

[12] Dai J., Ueda T., Sato Y. Unified analytical approaches for determining shear bond characteristics of FRP-concrete interfaces through pullout tests. Journal of Advanced Concrete Technology. 2006;4:133-45.

[13] Lu X., Teng J., Ye L., Jiang J. Bond–slip models for FRP sheets/plates bonded to concrete. Engineering structures. 2005;27:920-37.

[14] Lu X., Ye L., Teng J., Jiang J. Meso-scale finite element model for FRP sheets/plates bonded to concrete. Engineering structures. 2005;27:564-75.

[15] Dai J.-G., Ueda T. Local bond stress slip relations for FRP sheets-concrete interfaces. Fibre-Reinforced Polymer Reinforcement for Concrete Structures. Singapore: World Scientific; 2003. p. 143-52.

[16] Dai J.-G., Ueda T. A nonlinear bond stress-slip relationship for FRP sheet-concrete interface. The International Symposium on Latest Achievement of Technology and Research on Retrofitting Concrete Structures. Kyoto, Japan: Japan Concrete Institute; 2003. p. 107-12.

[17] López-González J.C., Fernández-Gómez J., González-Valle E. Effect of adhesive thickness and concrete strength on FRP-concrete bonds. Journal of Composites for Construction. 2012;16:705-11.

[18] Au C., Büyüköztürk O. Peel and shear fracture characterization of debonding in FRP plated concrete affected by moisture. Journal of Composites for Construction. 2006;10:35-47.

[19] Mazzotti C., Savoia M., Ferracuti B. A new single-shear set-up for stable debonding of FRP–concrete joints. Construction and Building Materials. 2009;23:1529-37.

[20] Cao S.Y., Chen J.F., Pan J.W., Sun N. ESPI measurement of bond-slip relationships of FRP-concrete interface. Journal of Composites for Construction. 2007;11:149-60.

[21] Zheng X.H., Huang P.Y., Chen G.M., Tan X.M. Fatigue behavior of FRP–concrete bond under hygrothermal environment. Construction and Building Materials. 2015;95:898-909.

[22] Raoof S.M., Bournas D.A. Bond between TRM versus FRP composites and concrete at high temperatures. Composites Part B: Engineering. 2017;127:150-65.

[23] Dai J., Ueda T., Sato Y. Bonding characteristics of fiber-reinforced polymer sheet-concrete interfaces under dowel load. Journal of Composites for Construction. 2007;11:138-48.

[24] Ueda T., Dai J. Interface bond between FRP sheets and concrete substrates: properties, numerical modeling and roles in member behaviour. Progress in Structural Engineering and Materials. 2005;7:27-43.

[25] Wu Z., Yuan H., Kojima Y., Ahmed E. Experimental and analytical studies on peeling and spalling resistance of unidirectional FRP sheets bonded to concrete. Composites Science and Technology. 2005;65:1088-97.

[26] De Lorenzis L., Miller B., Nanni A. Bond of fiber-reinforced polymer laminates to concrete. ACI Materials Journal. 2001;98:256-64.

[27] Pellegrino C., Tinazzi D., Modena C. Experimental study on bond behavior between concrete and FRP reinforcement. Journal of Composites for Construction. 2008;12:180-9.

[28] Alam M.S., Mandal A.B. Thermodynamic studies on mixed micellization of amphiphilic drug amitriptyline hydrochloride and nonionic surfactant Triton X-100. Journal of Molecular Liquids. 2012;168:75-9.

[29] Mukhtar F.M., Faysal R.M. A review of test methods for studying the FRP-concrete interfacial bond behavior. Construction and Building Materials. 2018;169:877-87.

[30] Al Azzawi M., Hopkins P., Mullins G., Sen R. FRP–Concrete Bond after 12-Year Exposure in Tidal Waters. Journal of Composites for Construction. 2018.

[31] Wang J. Cohesive-bridging zone model of FRP–concrete interface debonding. Engineering Fracture Mechanics. 2007;74:2643-58.

[32] Mara V., Haghani R., Harryson P. Bridge decks of fibre reinforced polymer (FRP): A sustainable solution. Construction and Building Materials. 2014;50:190-9.

[33] Cromwell J.R., Harries K.A., Shahrooz B.M. Environmental durability of externally bonded FRP materials intended for repair of concrete structures. Construction and Building Materials. 2011;25:2528-39.

[34] Dai J.-G., Gao W., Teng J. Bond-slip model for FRP laminates externally bonded to concrete at elevated temperature. Journal of Composites for Construction. 2013;17:217-28.

[35] Gao W., Teng J., Dai J.-G. Effect of temperature variation on the full-range behavior of FRP-to-concrete bonded joints. J Compos Constr. 2012;16:671-83.

[36] Li G., Pang S.-S., Helms J.E., Mukai D., Ibekwe S.I., Alaywan W. Stiffness degradation of FRP strengthened RC beams subjected to hygrothermal and aging attacks. J Compos Mater. 2002;36:795-812.

[37] Dai J., Kato E., Iwanami M., Yokata H. Durability of carbon strand sheet to concrete bond interface under moisture condition. Proceedings of The Fourth International Conference on FRP Composites in Civil Engineering. Zurich, Switzerland2008.

[38] Chajes M.J., Thomson Jr T.A., Farschman C.A. Durability of concrete beams externally reinforced with composite fabrics. Construction and building Materials. 1995;9:141-8.

[39] Toutanji H.A., Gómez W. Durability characteristics of concrete beams externally bonded with FRP composite sheets. Cem Concr Compos. 1997;19:351-8.

[40] Almusallam T.H. Load–deflection behavior of RC beams strengthened with GFRP sheets subjected to different environmental conditions. Cem Concr Compos. 2006;28:879-89.

[41] Sen R., Shahawy M., Mullins G., Spain J. Durability of Carbon Fiber-Reinforced Polymer/Epoxy/Concrete Bond in Marine Environment. ACI Structural Journal.96.

[42] Wang J.-z., Zhang J. Experimental study on bond performance between CFRP and concrete in seawater environment. Journal of Water Resources and Architectural Engineering. 2013;11:51-5.

[43] Al-Mahmoud F., Mechling J.-M., Shaban M. Bond strength of different strengthening systems – Concrete elements under freeze–thaw cycles and salt water immersion exposure. Construction and Building Materials. 2014;70:399-409.

[44] Silva M.A.G., Biscaia H. Degradation of bond between FRP and RC beams. Compos Struct. 2008;85:164-74.

[45] Zhang L., Jianxu M., Lin Z. Durability test of reinforced concrete structures externally bonded with CFRP in marine environment. China Civ Eng J. 2010;43:15951.

[46] Ashrafi H., Bazli M., Jafari A., Ozbakkaloglu T. Tensile properties of GFRP laminates after exposure to elevated temperatures: Effect of fiber configuration, sample thickness, and time of exposure. Compos Struct. 2020;238:111971.

[47] Liu T.Q., Liu X., Feng P. A comprehensive review on mechanical properties of pultruded FRP composites subjected to long-term environmental effects. Composites Part B Engineering. 2020;191:107958.

[48] Chu W., Wu L., Karbhari V.M. Durability evaluation of moderate temperature cured E-glass/vinylester systems. Compos Struct. 2004;66:367-76.

[49] Jansen K.M.B., Zhang M.F., Ernst L.J., Vu D.K., Weiss L. Effect of temperature and humidity on moisture diffusion in an epoxy moulding compound material. Microelectronics Reliability. 2020;107:113596.

[50] Kafodya I., Xian G., Li H. Durability study of pultruded CFRP plates immersed in water and seawater under sustained bending: Water uptake and effects on the mechanical properties. Composites Part B: Engineering. 2015;70:138-48.

[51] Pan J., Huang Y., Xing F. Effect of chloride content on bond behavior between FRP and concrete. Transactions of Tianjin University. 2010;16:405-10.

[52] Dai J.-G., Yokota H., Iwanami M., Kato E. Experimental Investigation of the Influence of Moisture on the Bond Behavior of FRP to Concrete Interfaces. Journal of Composites for Construction. 2010;14:834-44.

[53] Silva M., Biscaia H.C., Marreiros R.C. Bond–slip on CFRP/GFRP-to-concrete joints subjected to moisture, salt fog and temperature cycles. Composites Part B-engineering. 2013;55:374-85.

[54] Al-Tamimi A.K., Hawileh R.A., Abdalla J.A., Rasheed H.A., Al-Mahaidi R. Durability of the Bond between CFRP Plates and Concrete Exposed to Harsh Environments. Journal of Materials in Civil Engineering. 2015;27:04014252.

[55] Mukhopadhyaya P., Swamy R.N., Lynsdale C.J. Influence of aggressive exposure conditions on the behaviour of adhesive bonded concrete–GFRP joints. Construction and Building Materials. 1998;12:427-46.

[56] Hassan S.A., Gholami M., Ismail Y.S.B., Sam A.R.M. Characteristics of concrete/CFRP bonding system under natural tropical climate. Construction and Building Materials. 2015;77:297-306.

[57] Van Gemert D. Force transfer in epoxy bonded steel/concrete joints. International Journal of Adhesion and Adhesives. 1980;1:67-72.

[58] Kabir M.I., Shrestha R., Samali B. Effects of applied environmental conditions on the pull-out strengths of CFRP-concrete bond. Construction and Building Materials. 2016;114:817-30.

[59] Nguyen T.-C., Bai Y., Zhao X.-L., Al-Mahaidi R. Durability of steel/CFRP double strap joints exposed to sea water, cyclic temperature and humidity. Compos Struct. 2012;94:1834-45.

[60] Wu B., Zhang S., Liu F., Gan T. Effects of salt solution on mechanical behaviors of aramid fiber–reinforced polymer (AFRP) sheets and AFRP-to-concrete joints. Advances in Structural Engineering. 2016;19:1855-72.

[61] Yao J., Teng J.G., Chen J.F. Experimental study on FRP-to-concrete bonded joints. Composites Part B: Engineering. 2005;36:99-113.

[62] Robert M., Wang P., Cousin P., Benmokrane B. Temperature as an accelerating factor for long-term durability testing of FRPs: Should there be any limitations? Journal of Composites for Construction. 2010;14:361-7.

[63] Li J., Gravina R., Visintin P., Smith S.T. Durability and long-term performance of FRP-to-concrete joints under environmental conditioning: experimental and analytical study. Journal of Composites for Construction. 2020;24:04020021.